Cold Regions Science and Technology 194 (2022) 103435

Contents lists available at ScienceDirect

Cold Regions Science and Technology

journal homepage: www.elsevier.com/locate/coldregions

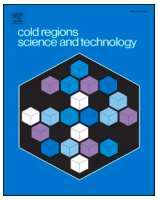

Performance quantification of icebreaker operations in ice management by numerical simulations

Jon Bjørnø [a,c,*], Marnix van den Berg [a,b], Wenjun Lu [a,b], Roger Skjetne [a,c], Raed Lubbad [a,b], Sveinung Løset [a,b]

[a] Sustainable Arctic Marine and Coastal Technology (SAMCoT), Norwegian University of Science and Technology (NTNU), Trondheim, Norway
[b] Department of Civil and Environmental Engineering, NO-7491 Trondheim, Norway
[c] Department of Marine Technology, NO-7491 Trondheim, Norway

ARTICLE INFO

Keywords:
Ice management operations
Simulation-based design
Ship-ice interactions
Image processing
Multi-body dynamics
Arctic technology
Ocean engineering

ABSTRACT

The paper addresses the problem of quantifying and assessing the effectiveness of icebreaker operations in ice management (IM) using a high-fidelity simulator. The numerical model includes an accurate geometric representation of an icebreaker, a cylindrical protected structure, and a synthetic ice environment. A set of key performance indicators (KPIs) are defined and proposed to quantify the effectiveness of IM strategies for protecting the downstream structure. This give better insight into which IM strategies are more effective with respect to different objectives for certain conditions, thereby enabling better planning and guidance of icebreaker operations.

The results from a selection of the simulations performed with nearly 100% ice concentration are presented. This will illustrate the methodology using the different KPIs to quantify the effectiveness and highlight differences between the different IM strategies. From the simulations we see that all patterns have strengths and weaknesses; some KPIs are consistent while others are changing with the ice drift velocity.

1. Introduction

The Arctic marine climate can be rough, and especially the presence of sea ice makes the design of offshore structures and marine operations highly complex. To reduce risk of stationkeeping operations in sea ice, ice management (IM) is often deployed, e.g., Molipaq and Kulluk in Canadian waters. Eik (2010) defined IM as the sum of all activities with the objective to reduce or avoid actions from any kind of ice features, where an IM system mainly consists of an ice observation system and a response system. *Sea ice management* is considered in this paper (as opposed to *iceberg management*), where the objective of the physical response system is to reduce the incoming sea ice into acceptable ice floes, using one or more icebreakers, such that the downstream protected structure (PS) is guarded from dangerous ice load levels.

Ice management is a comprehensive and integrated operation that involves detection, tracking, forecasting, decision making, and eventually handling the identified threatening ice features (ISO/FDIS/19906, 2019). Practical questions such as: "How many icebreakers are needed?" and "How to deploy the icebreaker fleet to effectively defend an offshore structure?" often occur when planning an IM operation. These are often addressed by empirical data and simplified models due to a limitation in ice surveillance (Lu et al., 2016b), limited detailed scientific data from

Abbreviations: IB, icebreaker; IM, ice management; KPI, key performance indicator; PS, protected structure; SAMS, Simulator for Arctic Marine Structures; DP, dynamic positioning, meaning thrusters are automatically controlled to keep station; OATRC'15, Oden Arctic technology research cruise 2015; ACEX, Arctic coring expedition; DOF, degree of freedom; FSD, floe size distribution; KPI-Work, icebreaker effort in terms of work; KPI-AMF, absolute mean force on protected structure; KPI-ILULR, impulse of loads under limit ratio (relative to the impulse of total loads) for the protected structure; KPI-ProdLoads, icebreaker production of loads on the protected structure not exceeding threshold over time; KPI-EffLoads, efficiency of the icebreaker to keep the loads on the protected structure below threshold relative to effort (work) spent; KPI-FSULR, floe size under limit ratio (relative to the total area of floes) after ice management; KPI-ProdFloes, icebreaker production of floes with sizes not exceeding threshold over time; KPI-EffFloes, efficiency of the icebreaker to produce floe sizes below threshold relative to effort (work) spent; KPI-ProdErrFloes, faulty production of floe sizes by the icebreaker; NED, North-East-Down reference frame.

* Corresponding author at: Sustainable Arctic Marine and Coastal Technology (SAMCoT), Norwegian University of Science and Technology (NTNU), Trondheim, Norway.

E-mail address: jon.bjorno@ntnu.no (J. Bjørnø).

https://doi.org/10.1016/j.coldregions.2021.103435
Received 20 October 2020; Received in revised form 20 August 2021; Accepted 5 November 2021
Available online 15 November 2021

earlier IM operations, and a lack of physics-based models to effectively characterize and predict the ice-structure interaction processes at operational scale (Lu et al., 2018a). As a reduced and efficient model, the kinematic model by Hamilton et al. (2011a,b) and Hamilton (2011) can be used. However, as technological advancements are improving, the retrieval of ice information in real time and the development of high-fidelity numerical models to estimate and predict time evolutions of both dynamic responses and internal loads between ice floes and structures are getting better; see for instance Heyn et al. (2017), Lubbad et al. (2018a,b), and Tsarau et al. (2018). Both the reduced models and high-fidelity numerical models have their strengths and weaknesses, so that the right model must be chosen according to the objective and desired outcome.

Most numerical methods target structural design, i.e., at the structural scale from a few meters to a few 100 meters. Detailed computational methods, such as the Finite Element Method (FEM), Discrete Element Method (DEM), and other computational methods have been applied to simulate the deformation and fracture of sea ice, and the subsequent ice accumulation; e.g., see the related review works (Lu, 2014) and (Tuhkuri and Polojärvi, 2018). When analyzing a system such as IM at operational scale, due to the large simulation domain (i.e., kilometers) and operation duration (i.e., hours), any computational mechanics-based numerical simulation becomes impractical due to the immense computational burden. Given the gap in concurrent simulation technology, the Simulator for Arctic Marine Structure (SAMS) has been developed to cope efficiently with numerical simulations in both the structural and operational scales (Lubbad et al., 2018b). SAMS is a mechanics-based simulator. It takes the mechanics during ice-structure interaction into account while maintaining simulation efficiency. SAMS applies the non-smooth DEM framework combined with an analytical formulation of ice fractures.

The main objectives and novelty of this paper is to quantify the performance of different IM strategies by defining a set of key performance indicators (KPIs) that are evaluated using high-fidelity simulation data – generated by configuring SAMS with icebreaker (IB) Oden, a cylindrical protected structure, and a synthetic ice environment. The KPIs are targeted mainly for design and operational planning, as there are inputs to the KPIs that cannot easily be measured during real operations. This will then demonstrate the capability of using mechanics-based models to numerically compute, with high-fidelity, icebreaker motions in different ice conditions. First, a problem formulation is presented where we detail the study and propose a set of KPIs as performance measures for ice load reduction by icebreakers. Then we present the simulation methodology with necessary background and details on the creation of the different parts of the simulations. Last, we run the simulations and analyze the results.

2. Problem formulation

We investigate the efficacy of icebreaker operations in IM. The problem is how to generate credible IM data and how to analyze the data to quantify the resulting performance of ice load reduction by the icebreaker operations. Quantifiable criteria for the performance of different IM patterns have typically been studied by evaluating the ice floe distributions resulting from a few real operations and from simplified kinematic icebreaking models. Using a high-fidelity simulation model, performance can be quantified by a richer set of parameters. In addition to the ice floe size information, we will also consider the ice loads on the protected structure, as well as the icebreaker effort, as criteria.

IB Oden was chosen as the IM vessel in this paper. The IB Oden, featured in Fig. 1, is the largest Swedish icebreaker with DNV Polar-20 class, owned and operated by the Swedish Maritime Administration. During the winter months, the icebreaker operates to clear a passage through the ice in the Gulf of Bothnia for cargo ships. In the summer, it serves as a research vessel for the Swedish Polar Research Secretariat.

Fig. 1. Icebreaker Oden. Photo: J. Bjørnø, 2016.

Since this icebreaker has been used extensively in research, with a significant amount of full scale data and digital geometric data existing, it has been chosen as case in this paper.

2.1. Ice management operation and icebreaking patterns

In sea ice management, an *ice load reduction system* is implemented in terms of one or more icebreakers to process the drifting sea ice in stages upstream the PS. Such a system can be considered as an industrial plant, working 24/7, to constantly process new incoming sea ice and reducing this into broken ice pieces with a size not exceeding a target threshold. The ultimate goal is to keep the loads on the PS under a specified load limits typically set based on the thrust capacity (for DP), mooring capacity, damage load conditions, etc., with operational safety factors added on top of that.

The width of the produced ice channel, setting the breadth of the chosen icebreaking pattern, is determined by the uncertainty in the ice drift forecast, especially forecasted changes in ice drift direction. Larger uncertainty implies a wider channel. High ice drift speeds, on the other hand, implies a narrower channel to ensure that the icebreaker manages to process all incoming ice and avoid that large floes escape its operation area. For safety-critical operations with high ice concentration, high drift speeds, and significant forecast uncertainties, more icebreaker stages must be considered. However, at higher drift speeds there is often less uncertainty in the forecast, whereas at lower speeds, or no drift at all, a much wider corridor must be planned to account for sudden changes in ice drift direction when the speed increases again.

Fig. 2 shows an example of a 2-stage IM setup, where a channel width based on the forecast has been determined. To account for the forecast uncertainty, a sector with angle $\alpha = 5 - 10$ degrees is normally added on each side as extra margin, giving a slightly wider effective ice channel. In the Oden Arctic Technology Research Cruise 2015 (OATRC'15) (Lubbad et al., 2018a), such a 2-stage IM operation was carried out as a full-scale trial in the Arctic sea ice north of Svalbard, as shown in Fig. 3. Each icebreaker was following a banana-shaped pattern, configured in 2 stages, to protect a virtual structure.

A ship-shaped PS is featured in Fig. 2, whereas a virtual point was used in OATRC'15. In our simulation-based analysis, the PS will be a cylindrical structure to serve as a measuring probe that will have a fixed position and can withstand all loads. Icebreaker Oden and the PS are placed in a synthesized ice field, with specified ice concentration, that aims to accurately mimic a real ice environment.

Four different ice management patterns will be evaluated in this study as shown in Fig. 4. These are circular track, racetrack, banana-shaped track (arced racetrack), and figure-8 track, where each pattern is made up from circles and line segments. Each track has parameters that can be adjusted, and the most critical parameters depend on the ice drift velocity, such as the target channel width, turning radius of IB

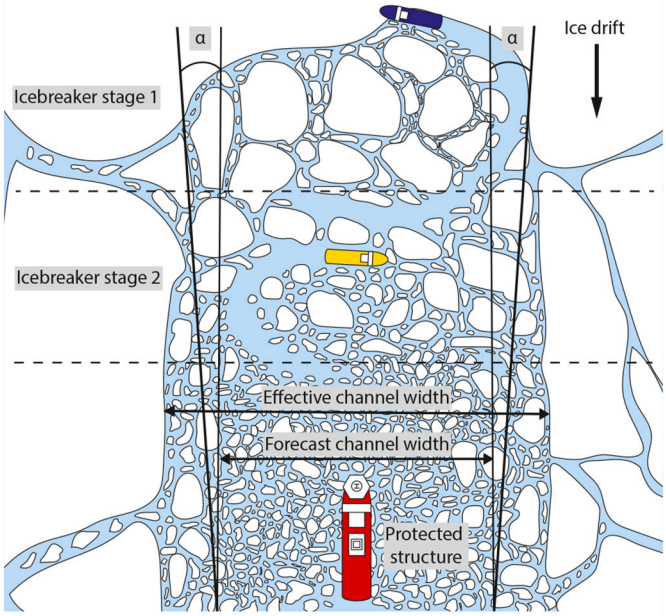

Fig. 2. The IM concept with channel width explanation.

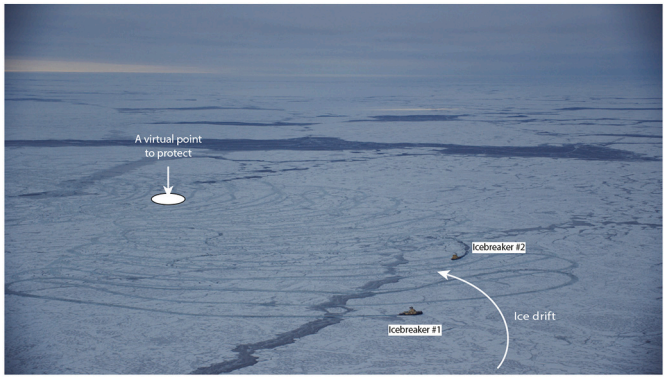

Fig. 3. IM field tests carried out during OATRC'15, with two icebreakers following banana-shaped patterns (perspective view, adapted from Holub et al., 2018). Photo: S. Løset, 2015.

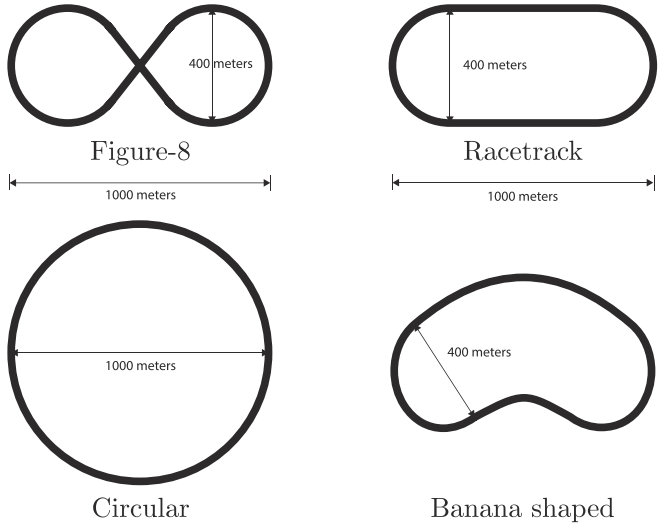

Fig. 4. Illustration of the different IM patterns tested.

Oden, etc. These parameters are kept constant during the different simulations. The icebreaker speed will be kept equal and constant for each pattern, which implies that the icebreaker speed is not limited by the maximum thrust capacity. This assumption will be discussed in Section 3.6.

2.2. Performance measures of physical ice management

When defining metrics to quantify icebreaker performance in an ice load reduction system, we can consider cost functions as KPIs, where lower is better. Alternatively, we can measure the performance by *productivity*, meaning production rate or produced output over time, or by *efficiency*, meaning the produced output vs. resources or effort spent. For productivity and efficiency, higher is better.

In several load-based KPIs, the load acting on the PS will be analyzed relative to a specified global force magnitude threshold $\overline{F}$. Similarly, floe-based KPIs will be assessed with respect to a specified size threshold $\overline{L}$ referred to as the "limit characteristic length" of the floes. This means that all floes below the limit are equally worth in terms of production success or failure (e.g., one floe of size 100 m^2 is in terms of production equally valuable as 10 floes of size 10 m^2), whereas in terms of efficiency, the one large but acceptable floe are likely more cost-efficient if this requires less energy to produce.

2.2.1. Parameters extracted from the simulation

More parameters are available from numerical simulations than can normally be obtained from real operations. The load and velocity vectors from the simulation model are in 6 degrees of freedom (DOF). We thus distinguish between translational and rotational modes by the load vector $\tau := (F, M)$ – where $F \in \mathbb{R}^3$ is the force and $M \in \mathbb{R}^3$ is the moment, and velocity $\nu = (v, \omega)$ – where $v \in \mathbb{R}^3$ is the linear velocity and $\omega \in \mathbb{R}^3$ is the rotational velocity. The parameters we consider are:

- Icebreaker Oden's velocity v_{IB}, global ice load τ_{IB}, power P_{IB}, and work W_{IB}. The hydrodynamic resistance is not considered as all simulations are performed with the same constant speed, thus the hydrodynamic resistance will not contribute to a more informative comparison of the ice management patterns.
- Ice force $F_{\mathrm{PS}} \in \mathbb{R}^3$ on the protected structure. From this we derive the mean force magnitude $F_{m,\mathrm{PS}} \in \mathbb{R}_{\geq 0}$, the significant force magnitude $F_{s,\mathrm{PS}} \in \mathbb{R}_{\geq 0}$, and the peak force magnitude $F_{p,\mathrm{PS}} \in \mathbb{R}_{\geq 0}$.
- Ice floe sizes, as processed by the icebreaker, in terms of characteristic length L_{floe} and area A_{floe}.
- Floe size distribution (FSD).

The peak ice forces in sea ice operations may contain significant energy levels, causing floating vessels to be pushed off position or causing damage to stationary structures. However, the highest peak force F_p may only cause small changes in momentum (for short time duration), whereas the average ice force typically underestimates the transient momentum changes of interest. Kjerstad et al. (2013) introduced the significant ice force magnitude $F_s \in \mathbb{R}_{\geq 0}$, defined as the average of the 1/3 largest force magnitudes, as a measure of a representative global force level to use in capability analysis of stationkeeping in sea ice by dynamic positioning. As an alternative, however, we consider the momentum of the ice load and introduce a parameter calculated by the integral of the force magnitude $|F|$ with respect to time, i.e., the "impulse of force magnitude" $I(t) = \int_{t_0}^{t} |F(\sigma)| d\sigma$ where $|\cdot|$ is the vector 2-norm. Since the simulation runs in discrete time with fixed time step ΔT, where the force is constant during each step, this quantity is calculated by the sum

$$I(t_k) = \sum_{j=0}^{k-1} |F(t_j)|\Delta T = I(t_{k-1}) + |F(t_{k-1})|\Delta T, \qquad I(t_0) = 0, \tag{1}$$

where $t_k = t_{k-1} + \Delta T$ for $k = 1, 2, 3, \ldots$.

Other important parameters are the consumed power P and applied work W by a vessel moving in ice. Given a corresponding velocity vector ν and total load τ, the power and work are calculated as $P(t) = \tau(t)^\top \nu(t)$ and $W(t) = \int_{t_0}^{t} P(\sigma)d\sigma$. As for the impulse, the work is calculated by the sum of discrete values,

$$W(t_k) = \sum_{j=0}^{k-1} P(t_j)\Delta T = W(t_{k-1}) + P(t_{k-1})\Delta T, \qquad W(t_0) = 0. \tag{2}$$

This will be used to monitor the effort or resources spent by the icebreaker to produce a broken ice field.

2.2.2. Performance metrics

Considering cost functions to quantify performance, it is immediate to consider the effort put into work by the icebreaker as well as the loads on the PS. In addition, we will consider floe production of the icebreaker in terms of floe sizes not exceeding a given limit.

2.2.2.1. Icebreaker effort. A KPI we monitor is the icebreaker's effort put into icebreaking in terms of the work (2) due to the ice load from t_0 to t_k, that is (3).

$$\text{KPI-Work} \quad W_{\text{IB}}(t_k) = W_{\text{IB}}(t_{k-1}) + \tau_{\text{IB}}(t_{k-1})^\top \nu_{\text{IB}}(t_{k-1})\Delta T, \quad W_{\text{IB}}(t_0) = 0. \tag{3}$$

2.2.2.2. Loads on protected structure. Since the PS is cylindrical, we neglect the moments and only consider the global force vector $F_{\text{PS}}(t)$. Hence, we quantify the absolute mean force (AMF) by the KPI in (4).

$$\begin{aligned}\text{KPI-AMF} \quad F_{m,\text{PS}}\left(t_k\right) &= \frac{1}{k+1}\sum_{j=0}^{k} |F_{\text{PS}}\left(t_j\right)| \\ &= \frac{k}{k+1} F_{m,\text{PS}}\left(t_{k-1}\right) + \frac{1}{k+1}|F_{\text{PS}}\left(t_k\right)|.\end{aligned} \tag{4}$$

To address the change in momentum due to the force peaks exceeding the threshold $\overline{F}$, we monitor two parameters. One is the impulse due to the force magnitude $|F_{\text{PS}}(t)|$ when this is saturated by $\overline{F}$, denoted by $I_{\text{loads}\le\overline{F}}(t_k)$. This will be compared to the impulse of the total unsaturated magnitude force, denoted $I_{\text{tot}}(t_k)$. Both are calculated as in (1), but with force saturated in the former signal. The KPI for change in momentum for the PS is then proposed as "Impulse of Loads Under Limit Ratio" (ILULR) in (5).

$$\text{KPI-ILULR} \quad M_{\text{loads,PS}}\left(t_k\right) = \frac{I_{\text{loads}\le\overline{F}}(t_k)}{I_{\text{tot}}(t_k)} \in \left[0, 1\right], \quad M_{\text{loads,PS}}\left(t_0\right) := 1. \tag{5}$$

If all load magnitudes stay below $\overline{F}$ from t_0 to t_k, then $M_{\text{loads,PS}}(t_k) = 1$, whereas load peaks exceeding the threshold will result in a number below 1. The area of such exceeding load peaks is thus quantified by the ratio $\frac{I_{\text{tot}}(t_k) - I_{\text{loads}\le\overline{F}}(t_k)}{I_{\text{tot}}(t_k)} = 1 - M_{\text{loads,PS}}(t_k)$.

For "load production" we consider the amount of time that the load magnitudes on the PS are kept below the threshold load $\overline{F}$. Letting $N_{\text{loads}\le\overline{F}}(t_k)$ be the count of sample periods that $|F_{\text{PS}}(t_k)| \le \overline{F}$ is satisfied from t_0 to t_k, then the amount of time is given by $T_{\text{loads}\le\overline{F}}(t_k) = N_{\text{loads}\le\overline{F}}(t_k)\Delta T$. Based on this, the productivity Π and efficiency Ω of the ice load reduction system with respect to loads on the PS are proposed as (6) and (7).

$$\text{KPI-ProdLoads} \quad \Pi_{\text{loads}}\left(t_k\right) = \frac{T_{\text{loads}\le\overline{F}}(t_k)}{t_k}, \quad \Pi_{\text{loads}}\left(t_0\right) := 0, \tag{6}$$

$$\text{KPI-EffLoads} \quad \Omega_{\text{loads}}\left(t_k\right) = \frac{T_{\text{loads}\le\overline{F}}(t_k)}{W_{\text{IB}}(t_k)}, \quad \Omega_{\text{loads}}\left(t_0\right) := 0. \tag{7}$$

Note that $\Pi_{\text{loads}}(t_k) \in [0, 1]$ where 1 means perfect icebreaking with respect to load levels, whereas $1 - \Pi_{\text{loads}}(t_k)$ is the ratio of time durations of load magnitudes exceeding $\overline{F}$.

2.2.2.3. Ice floe sizes. We consider as a KPI the ratio of accumulated area of floes below the specified size threshold $\overline{L}$ compared to the total ice area drifting in the channel. To measure only floes within a reasonable channel affecting the PS, we define a *KPI evaluation corridor* by the two vertical lines shown in Fig. 5, having width D less than the effective channel width and centerline at the PS. By doing this we avoid counting partly broken large floes drifting in the boundary region of the icebreaking channel. As indicated in Fig. 5, we also define two horizontal lines for logging 1) the incoming ice to the icebreaking area, and 2) the produced ice leaving the area. From this, only floes with geometrical center passing the produced ice log line and within the KPI evaluation corridor, will be measured with respect to their sizes. However, two issues must be accounted for when considering the size-based KPIs:

1. The simulation model removes brash ice pieces below a certain size to make computations more efficient. The area of these pieces must also be counted into the KPIs.
2. Depending on the icebreaker path/pattern, large floes may be pushed either dominantly to the center of the icebreaking channel or to the sides of the channel. Icebreaker patterns that push large floes mainly outside the KPI evaluation corridor should be favorably rewarded in the KPI compared to patterns placing large floes mainly within the evaluation corridor.

To account for these effects, we cannot strictly count sizes of floes below $\overline{L}$ within the corridor. Instead, we count the large floes exceeding $\overline{L}$ and then subtract this from the total incoming ice area. The resulting accumulated area will then account for brash ice pieces, floes below $\overline{L}$, and also new area of water leads that are opened by the icebreaker.

To compute the total incoming ice area within the KPI evaluation corridor, we can for each sample calculate the area of the new ice that has passed the incoming ice log line. However, as we know the ice concentration C_{ice} of the entire ice cover as set in the ice field synthesis, we can use this to simplify the calculation – assuming C_{ice} will be the average concentration of incoming ice over time. The new area of ice passing the incoming ice log line for each sample is then $C_{\text{ice}} D v_{\text{ice}} \Delta T$, so

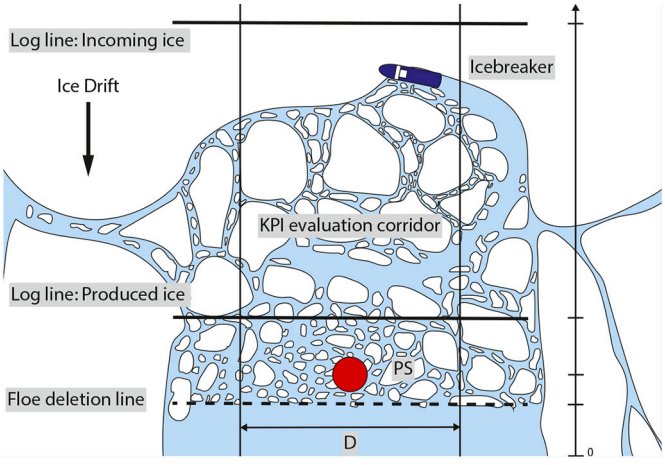

Fig. 5. Illustration of the different lines used for the purpose of performance quantification when evaluating the results of an IM simulation.

that the accumulated total area becomes as (8).

$$A_{\text{tot}}(t_k) = C_{\text{ice}} D v_{\text{ice}} (t_k - t_0) = A_{\text{tot}}(t_{k-1}) + C_{\text{ice}} D v_{\text{ice}} \Delta T, \quad A_{\text{tot}}(t_0) := 0, \tag{8}$$

where C_{ice}, D, v_{ice}, and ΔT are constants in the simulation.

Let $A_{\text{floes}>\bar{L}}(t_k) = \sum A_{\text{floe}}|_{L_{\text{floe}}>\bar{L}}$ denote the accumulated area of floes that exceed $\bar{L}$ when these pass the produced ice log line within the KPI evaluation corridor. The KPI "Floe Size Under Limit Ratio" (FSULR) is then proposed as (9).

$$\text{KPI-FSULR} \quad R_{\text{floes}}\left(t_k\right) = \frac{A_{\text{tot}}(t_k) - A_{\text{floes}>\bar{L}}(t_k)}{A_{\text{tot}}(t_k)} \in \left[0,1\right], \; R_{\text{floes}}\left(t_0\right) := 1, \tag{9}$$

where $R_{\text{floes}}(t_k) = 1$ means perfect icebreaking from t_0 to t_k with respect to floe sizes. It follows that $1 - R_{\text{floes}}(t_k)$ is the ratio of floe sizes exceeding the threshold $\bar{L}$.

When assessing production Π, we consider the accumulated acceptable floe areas over time. Efficiency Ω, on the other hand, is the accumulated acceptable floe areas relative to icebreaker effort. Hence, we will measure the productivity Π and efficiency Ω of the ice load reduction system with respect to floe sizes by (10) and (11).

$$\text{KPI-ProdFloes} \quad \Pi_{\text{floes}}\left(t_k\right) = \frac{A_{\text{tot}}(t_k) - A_{\text{floes}>\bar{L}}(t_k)}{t_k}, \quad \Pi_{\text{floes}}\left(t_0\right) := 0, \tag{10}$$

$$\text{KPI-EffFloes} \quad \Omega_{\text{floes}}\left(t_k\right) = \frac{A_{\text{tot}}(t_k) - A_{\text{floes}>\bar{L}}(t_k)}{W_{\text{IB}}(t_k)}, \quad \Omega_{\text{floes}}\left(t_0\right) := 0. \tag{11}$$

Having defined the production KPI, we may also quantify the faulty production in terms of floe sizes exceeding the threshold, according to (12).

$$\text{KPI-ProdErrFloes} \quad \Gamma_{\text{floes}}\left(t_k\right) = \frac{A_{\text{floes}>\bar{L}}(t_k)}{t_k}. \tag{12}$$

3. Simulation methodology

3.1. Baseline: kinematic simulation model

The ice floe size distribution results, based on a kinematic approach, will be used as the baseline. The kinematic model has been widely applied in engineering practice, e.g., Hamilton et al. (2011a). The basic idea behind this model is that the icebreaking vessel is predefined to follow a certain icebreaking pattern in accordance with its icebreaking capability, i.e., h-v curves depending on the ice thickness. The broken floe size is assumed to be the same as the icebreaking channel spacing. Depending on different icebreaking patterns, different downstream floe size distributions are thus available. The kinematic method can be computationally efficient due to its simplifying assumptions. However, this method cannot be used to quantify the ice loads on the protected structure.

3.1.1. Extracting the floe sizes

The ice management patterns illustrated in Fig. 4 are utilized, following the kinematic approach to derive the downstream floe size distribution. The method is based on image processing (Toyota et al., 2006; Lu et al., 2008; Zhang and Skjetne, 2015). The work flow is presented in Fig. 6 using the figure-8 IM pattern as an example.

At first, given the drift direction and velocity (i.e., 0.2 m/s), the IM track over ice can be plotted in the left of Fig. 6 (to save space the full track is not plotted). Afterwards, based on image processing, different 'intact ice floes' that were intersected by the IM track were isolated in the middle of Fig. 6. The color scheme is based on the relative size of the ice floes with red to green indicating large to small ice floes. However, both field observations (Hamilton et al., 2011a; Lu et al., 2016a) and theoretical studies (Lu et al., 2015, 2018b,c) indicate that long cracks

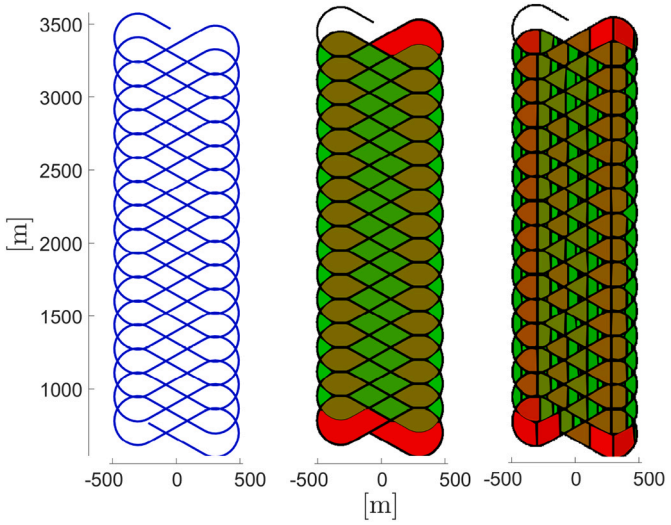

Fig. 6. Work-flow to extract the ice floe size distribution based on the kinematic IM approach. The larger floes at the beginning and end are removed, and only the produced floes over the continuous middle section are considered in the floe analysis.

form in between these IM track channels. These long cracks effectively lead to further floe size reductions. In this method, we adopt the same assumption as by Hamilton et al. (2011a) that the produced floe size follows a 1:1 ratio with the channel spacing. Given this assumption, we can introduce additional 'long cracks' in between different channels based on the spacing. Thus, the right figure in Fig. 6 is produced with ice floes of varying sizes produced in between the different channels. Finally, the floe size distribution can be extracted without the larger ice floes in the beginning and end. The results are presented with the characteristic ice floe length in Section 4.

3.2. Simulator for Arctic Marine Structures

A complete kinematic and dynamic simulation model yields, among many outputs, the downstream floe size distribution, the influence of the dynamics (drifting) of the ice floes created by ice management, and also the ice loads encountered by the icebreaker and the protected structure. By using high-fidelity simulators, all these parameters are available. A brief introduction to SAMS with validation studies is presented next.

SAMS is a numerical simulator intended for the simulation of interaction between sea ice and structures. It can simulate the motions, collisions, and failures of ice floes and structures. The ice floe environment in SAMS can be in the order of kilometers, where the ice floes can act as level ice or as smaller ice floes down to ice rubble blocks. SAMS uses the discrete element method (DEM) to determine the contact forces between bodies. These are calculated in each time step, where the ice material properties, the contribution of non-contact forces, and the influence of forces at other contacts are considered. Because of the computational efficiency inherent from the non-smooth DEM and analytical fracture algorithm, SAMS is capable of simulating large spatial and temporal domains. This enables SAMS applications within both Arctic offshore structural design (in the scale of hundreds of meters) and Arctic marine operation (in the scale of tens of kilometers).

Before SAMS was utilized in the current paper's simulation tasks, several validation studies were carried out. These include full-scale ship transit in a broken ice field (Lubbad et al., 2018a), comparison against the icebreaker Oden's performance (i.e., h-v curve) in level ice (Raza et al., 2019), multi-leg jacket type structure in model ice tests (van den Berg et al., 2019), and moored conical structure in model ice tests (Tsarau et al., 2018). The results of previously conducted validation studies show that SAMS is suitable for the IM simulations in this study.

More information about SAMS and more validation cases can be found in van den Berg et al. (2021).

3.3. Structures

3.3.1. IB Oden

The geometric model of IB Oden was accurately digitized from drawings using software packages that are free to use, such as *Blender* (Blender Foundation, 2018) and *DELFTShip Free* (DELFTShip Maritime Software, 2018). The input model of IB Oden contains 35 convex objects, which in total contains 2,240 vertices, 6,510 edges, and 4,338 faces. The large number of elements in the model allows a detailed approximation of IB Oden's hull, as seen in Fig. 7 with main dimension given in Table 1.

3.3.2. Protected structure

The geometry of a simple cylinder is made in *Blender*. It has a diameter of 70 meters, draft of 50 meters, and height above water level of 50 meters. The input model of the cylinder contains a single convex object, which in total contains 64 vertices, 96 edges, and 34 faces. During the simulations the cylinder will be fixed at a specified position. The cylinder is illustrated in Fig. 8.

3.4. Ice environment

A 12,000 meters by 3,000 meters computational domain is used to model the ice field. This is generated using a MATLAB® script. To achieve confinement, the domain has zero-friction tank walls. This can cause bridging effect between the tank wall and the structures, but with a wide enough tank area this effect is not present in this study. Both the icebreaker and the protected structure are located in open water at the start of the simulations. This is achieved by deleting the ice floes in the initial positions of the icebreaker and the protected structure. The script contains a set of parameters that are changed according to desired values to create an ice field with nearly 100% ice concentration, where the number of seed points determines the number of floes and (indirectly) the floe sizes. In this case we used 120 seed points. The Voronoi tessellation method is used to subdivide the ice domain into separate ice floes. After being generated, the ice field is exported with a homogeneous ice thickness. The resulting ice field, consisting of ice floes with a mean characteristic length of 476 meters, can be seen in Fig. 9, where the smaller ice floes ensures minimal removal at initialization. The main ice parameters set for SAMS are listed in Table 2.

3.5. Setup

The following simulation setup has been applied:

- The parameters for the ice field are; ice thickness h of 1.7 meters, ice concentration $C_{\text{ice}}\approx 100\%$, and constant ice drift v_{ice} that increases with increments of 0.1, from 0.1 m/s to 0.3 m/s, for each simulation. The ice drift speed has a limited variability since the ice thickness h is close to the limitation of IB Oden ($h_{\max} = 1.9$ m) and the use of only one icebreaker.

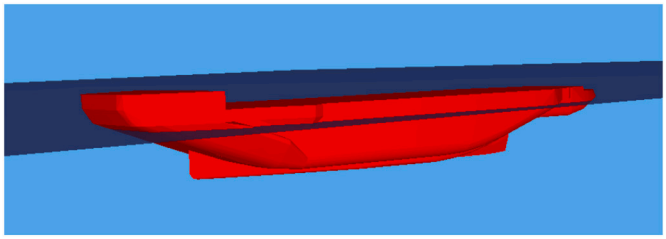

Fig. 7. The model of Oden.

Table 1
Technical data of Oden.

Length over all	107.75 meters
Beam	31.2 meters
Draft	8.5 meters
Displacement	13,000 tonnes

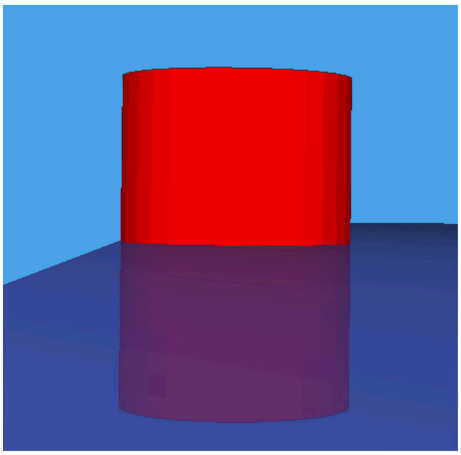

Fig. 8. The cylindrically shaped protected structure.

- The icebreaker will follow the four different IM patterns presented in Section 2.1, and perform these with constant speed according to the h/v-curve in Fig. 11, that is $v_{\text{IB}} = 3.882$ knots. The width of the IM channel is fixed and set to 1,000 meters, as also used in Hamilton et al. (2011b). This is normally set according to the ice drift forecast with additional breadth added according to the forecast uncertainties; see Section 2.1.
- The load criteria are determined by experts, typically taking into account the thrust capacity (for DP), mooring capacity, damage load conditions, etc., of the protected structure, with operational safety factors on top of that. As we only consider the global ice load in this study (see van den Berg et al. (2019), for a study of local loads), the load threshold will be set to $\overline{F} = 5$ MN in our study. To put this into perspective, Kulluk had a drilling limit of 750 tonnes (7.355 MN) (Palmer and Croasdale, 2012). The ice floe size criterion is also related to the capacity of the protected structure, with a safety margin. Two examples on this limit are ACEX 2004 (Backman et al., 2004) and Hamilton et al. (2011b), with 25 meters and 100 meters, respectively. Both of these are two stage IM operations, whereas we only study a single stage. Using the information given in those two sources, we increase the ice floe limit to $\overline{L} = 150$ meters due to thicker ice, resulting in lower icebreaker velocity, and only using a one stage IM operation. The threshold criteria are set such that the KPI values give an informative comparison between the different patterns for the simulated conditions.
- The logging width D of the KPI evaluation corridor, see Fig. 5, is set to be 9 times the diameter of the PS, that is, a total logging width of 630 meters within the IM channel.
- To keep the ice floes confined and not drifting to the sides we made two confinement/deletion criteria. The first one is related to ice drift velocity, where the ice floes keep a constant velocity above 3,000 meters and below 0 meter. The second criteria is related to deletion of ice floes, where the top point of each floe has to pass the deletion line before being deleted. See Fig. 10.

All of these limits are here set as an example to present the different KPIs. The limits will normally be set according to the actual IM operation planned for, based on prestudies such as presented in this paper. The

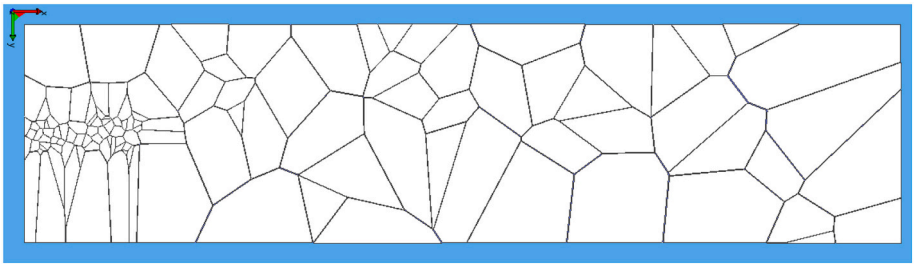

Fig. 9. An illustration of the ice field, with ice concentration ~100% and ice thickness 1.7 meters.

Table 2
SAMS global constant ice field parameters.

Parameters	Value
Ice density	910.0 [kg/m^3]
Crushing specific energy	2.0 [MJ/m^3]
Young's modulus	2.0 [GPa]
Poisson ratio	0.3 [–]
Damping coefficient ice-water	0.01 [–]
Fracture toughness	150 [kPa/m]
Flexural strength	2.0 [MPa]
Tensile strength	2.0 [MPa]
Friction coefficient ice-ice	0.15 [–]
Friction coefficient ice-structure	0.15 [–]
Friction coefficient ice-walls	0.0 [–]

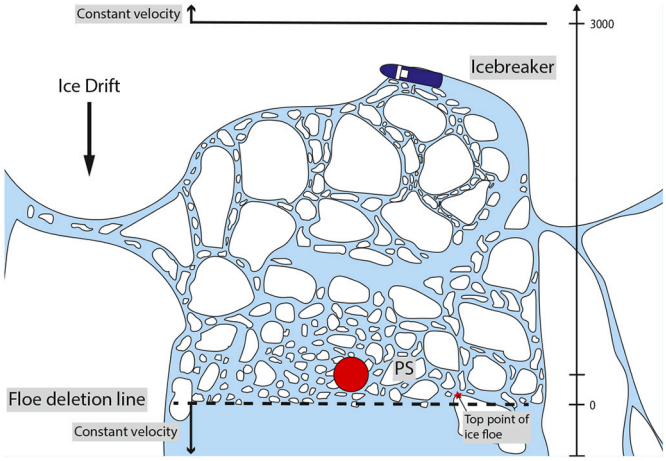

Fig. 10. Conceptual illustration of the confinement criteria used in the simulation.

simulations are stopped when they have reached a point with 4 hours of usable data. In addition, all floes passing the floe deletion line, see Fig. 5, will be removed to speed up computations.

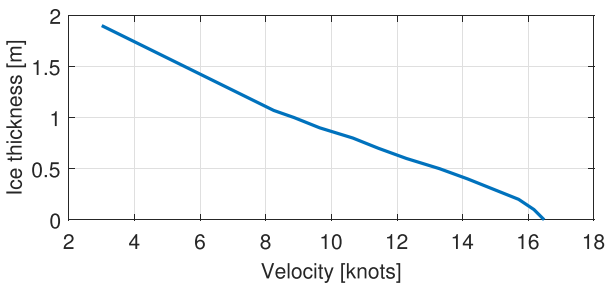

Fig. 11. The h/v curve for Oden. Courtesy of Johansson and Liljestrom (1989) and Swedish Maritime Administration (2013).

3.6. Assumptions and limitations

The icebreaker, including its speed and maneuverability, are often the limiting factor when solving IM challenges. During the simulations, IB Oden will be strictly following a predefined path at a given speed. This means that IB Oden is rigidly fixed (towed along the track at constant speed) and not free-floating. It will also maintain its constant speed while turning. This makes the study of the effect of ice breaking patterns on the ice cover more deterministic, at the cost of making the dynamic performance of the icebreaker less realistic. Hence, the limiting factors (feasibility) of the icebreaker itself will not be addressed directly in this study.

There is only one protected structure used as a "measuring prob" for the ice load. This can lead to situations where significant ice floes are not hitting the structure. The ice loads depend on if small or large ice floes hit the structure or not. This introduces randomness to the simulations. However, the setup used is in accordance with practice, where the effect of randomness is reduced by increased simulation length.

In real operations, the ice drift velocity varies with time. Here, the drift direction and speed are kept constant for each simulation, and only the speed is changed between simulations. This helps to ensure more deterministic results that are easier to compare afterwards.

To reduce simulation time, the protected structure is moved up from the original position at [0,0,0] to [50,0,0] in the NED-frame. This will give a relative distance of 325 meters to the bottom of the IM patterns. In real operations, this distance is normally larger, typically from 500 meters to several kilometers. In addition, the ice floes are deleted when their top point nearest to the PS is at 0 meter, that is, 50 meters behind the protected structure; see Fig. 5.

For each simulation, the initial time t_0 has been defined from a time instance when the original ice edge has drifted beyond the PS and become deleted, at which time the IM has reached a steady operating condition. All KPIs are evaluated and plotted from this initial time t_0.

4. Performance anazlysis

4.1. Floe size distributions

Plots from the kinematic analysis presented in Section 3.1 and simulation results from SAMS, with ice drift 0.20 m/s, are shown for each track in Fig. 12.

The kinematic results in Fig. 12 show an efficient way of plotting the floe sizes from the different patterns. By plotting the FSDs as in this figure, the effect of each pattern on the floe sizes is clearly distinguishable, as compared to the normal ice FSD histograms. It can be seen in the high-fidelity simulations that three patterns provide similar results on the production of ice floes, while the banana pattern sticks out. In the kinematic approach, the FSDs are more spread. We can also see that many more ice floes are present in the high-fidelity approach compared to the kinematic approach. These floes originate from the interaction mechanics, the ice breaking patterns, and the type of ice environment. In

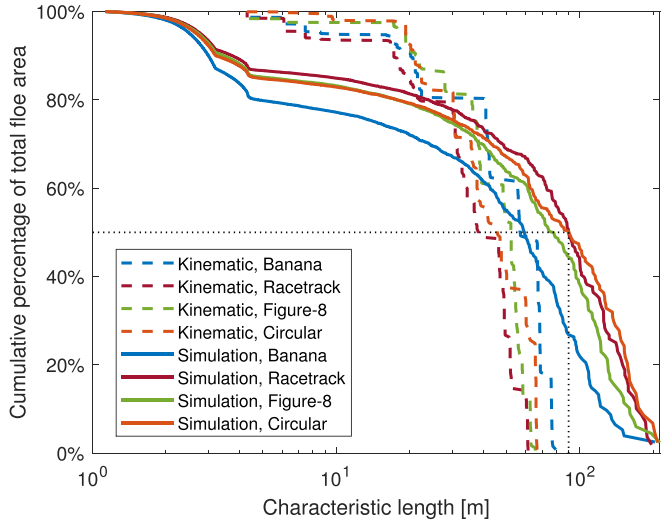

Fig. 12. Floe size results for $v_{ice} = 0.20$ m/s. Example reading of plot: 50% of the total ice floe area is above ~89 meters for the racetrack pattern.

the kinematic approach, the entire ice field is static level ice, and no ice fractures other than those produced by the track itself and the parallel channel heuristic mechanisms are used to generate the floes. In the high-fidelity approach, the ice field is dynamic, where the ice floes move around with ~100% ice concentration and fractures are formed by a number of mechanics-based analytical solutions. Contrary to the initial level ice sheet for the kinematic approach, the high-fidelity simulations start from a set of very large ice floes that make up the ice field, which next is broken into smaller ice floes, as reflected by the FSDs in Fig. 12. The motivation of using load-based KPIs in addition to assessment of the floe sizes is to get a clearer view in how the patterns differentiate.

4.2. KPI results

Plots from the different KPIs are presented one by one for three ice drift speeds, 0.10 m/s, 0.20 m/s, and 0.30 m/s. All plots are shown as time series.

4.2.1. KPI-Work

The KPI-Work measures the effort to perform the different patterns, as seen in Fig. 13. The difference between the patterns may seem small at times, but the difference seems to increase when the ice drift velocity increases. These differences can result from how often the IB hits the ice and how large these impacts are. In real operations, this indicator may be based upon the power produced by the machinery and power system, and will thus include also the hydrodynamic and inertial loads.

4.2.2. KPI-AMF and KPI-ILULR

Fig. 14 shows the KPI-AMF results, which clearly distinguish the mean load performance resulting from the different simulated patterns. Ice loads above or below the last mean value may slowly increase or decrease the KPI value. However, KPI-AMF will not quantify very large load peaks and how long these last. Such large load peaks can be critical, with consequences such as broken mooring lines or loss of position for the protected structure. In real operations, ice load measurements on the PS are needed to evaluate the KPI-AMF, e.g., by measuring the mooring tensions.

The KPI-ILULR is shown in Fig. 15. This KPI quantifies better the ice load peaks that contain significant energy. How long and steep the drops in the curve are, indicate the size and duration of the ice load peaks. An issue to be aware of, is that it will give steep drops in the beginning if an ice load peak is present initially. This issue is reduced by avoiding the initial transients in the evaluation of the KPIs. To use this KPI, the global load measurements need to be available in real operations.

4.2.3. KPI-ProdLoads and KPI-EffLoads

Fig. 16 shows the KPI-ProdLoads, that is, the portion of the operation time that the ice loads stay below the threshold. We observe that the circular pattern becomes worse with increasing drift velocity while the

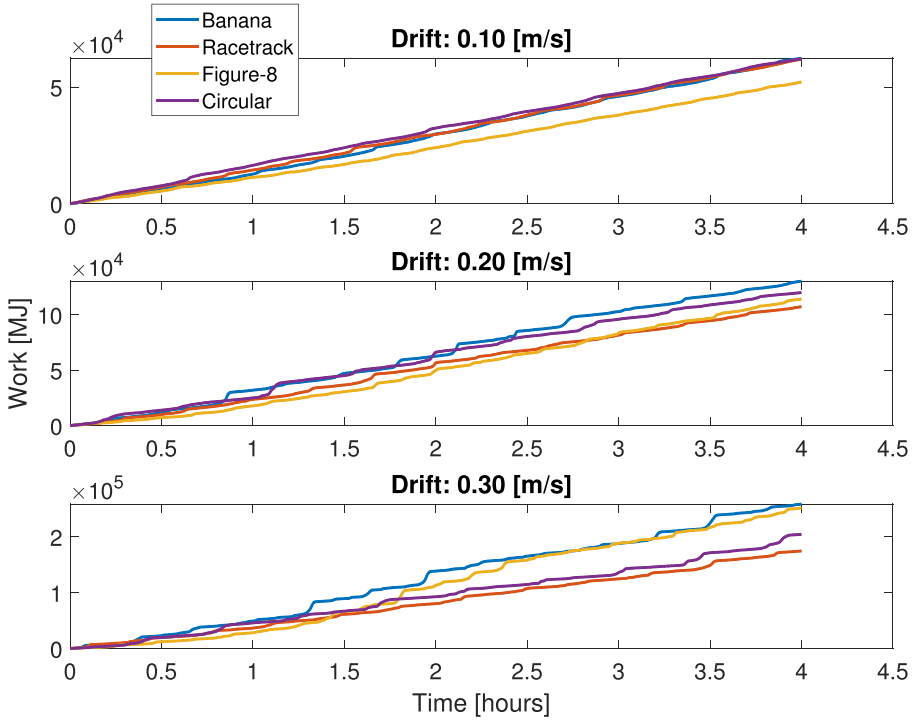

Fig. 13. KPI-Work.

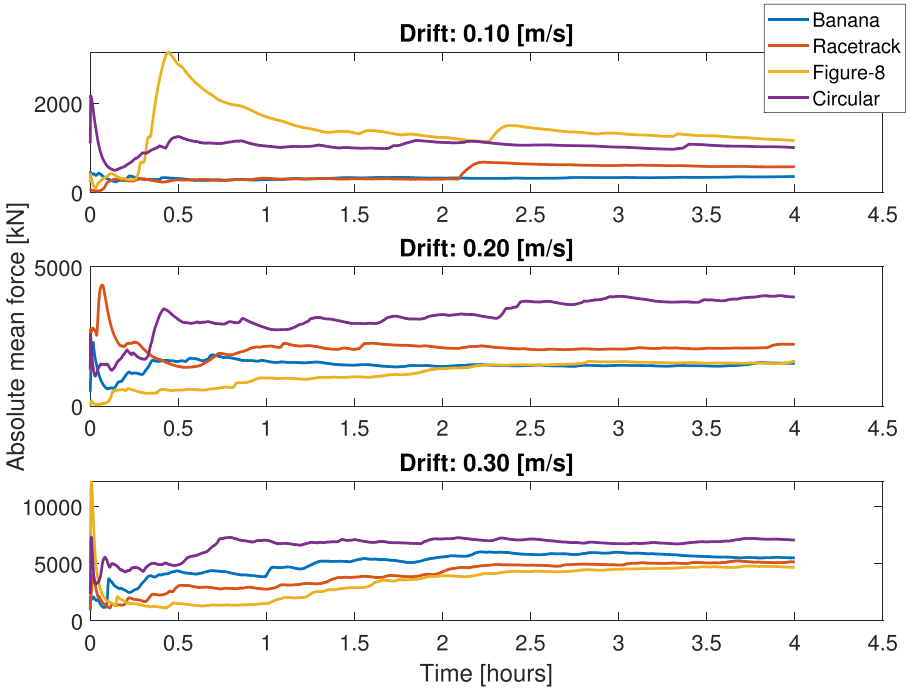

Fig. 14. KPI-AMF (lower value is better).

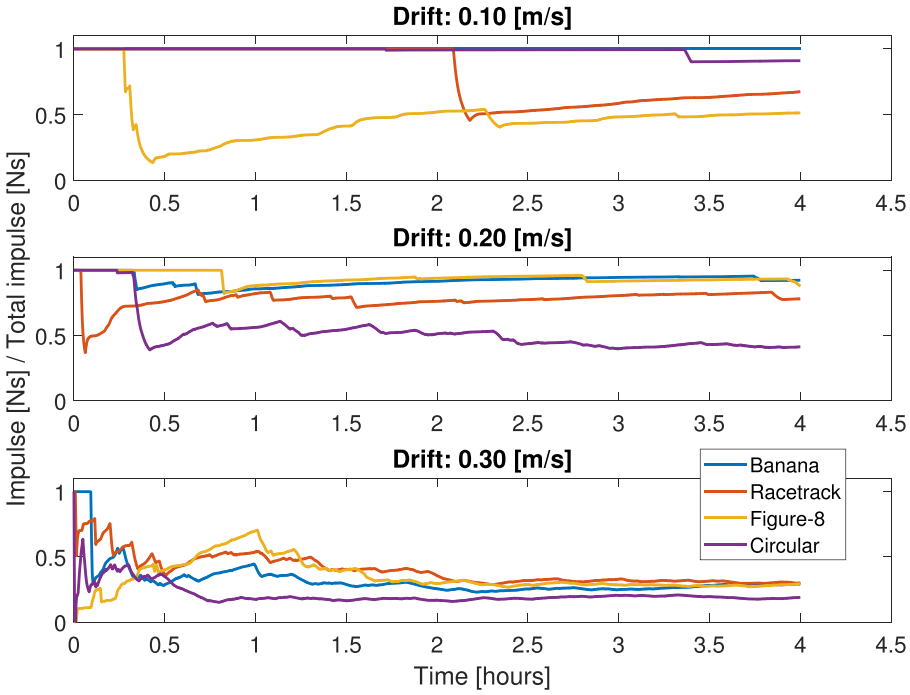

Fig. 15. KPI-ILULR (higher value is better).

figure-8 pattern becomes better. This KPI also suffers in the initial phase of the simulation and should not be measured before steady operation is reached, after which it will also attain a somewhat steady production.

The KPI-EffLoads is shown in Fig. 17. This KPI compares the efficiency of the different patterns in terms of load production per energy unit of the icebreaker. For load efficiency, we observe that there are variations between which pattern does better or worse. The racetrack and figure-8 pattern, however, seem as a trend to have better efficiency. To apply these KPIs in real operations, measurements of the icebreaker energy consumption together with the global loads for the protected structure are needed.

4.2.4. *KPI-FSULR*

The KPI-FSULR, shown in Fig. 18, indicates if there are too large floes produced by the IM. As for the KPI-ILULR, the steepness of drops in the curve has a meaning. Each drop gives an indication of the size or sizes of ice floes above threshold that slips through. Note also from the figure, for higher drift speeds, that there is a significant portion of produced

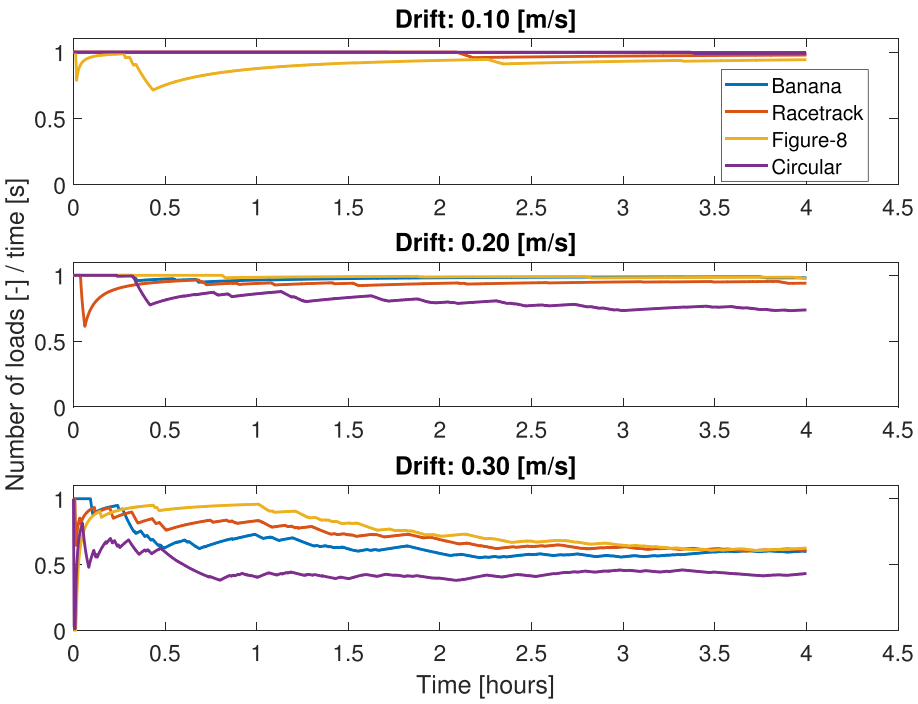

Fig. 16. KPI-ProdLoads (higher value is better).

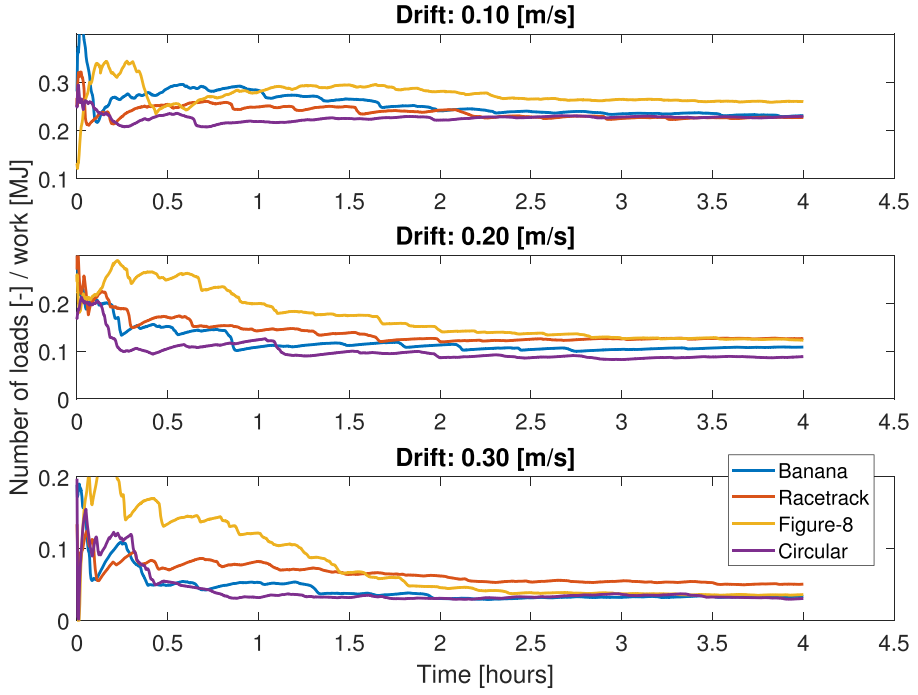

Fig. 17. KPI-EffLoads (higher value is better).

floes above the threshold. These result from the forced icebreaker motions simulated in this study, as the icebreaker cannot deviate from the fixed path. An increasing KPI-FSULR implies successful production of floe sizes, whereas decreasing implies that too large floes slip through. This KPI also has an initialization issue, where large floes in the beginning of the data series can results in huge drops due to lack of initial data points and transient effects. Hence, again it is important to start measuring when steady operation has been reached. In order to apply the KPI-FSULR in real operations, a floe size detection system should be implemented.

4.2.5. *KPI-ProdFloes and KPI-EffFloes*

Fig. 19 shows the KPI-ProdFloes, which gives an overview of the production of floes with acceptable sizes, that is, the produced area of acceptable floes over time. Here we see that the banana pattern shows the best performance for all drift velocities. However, it is not the most

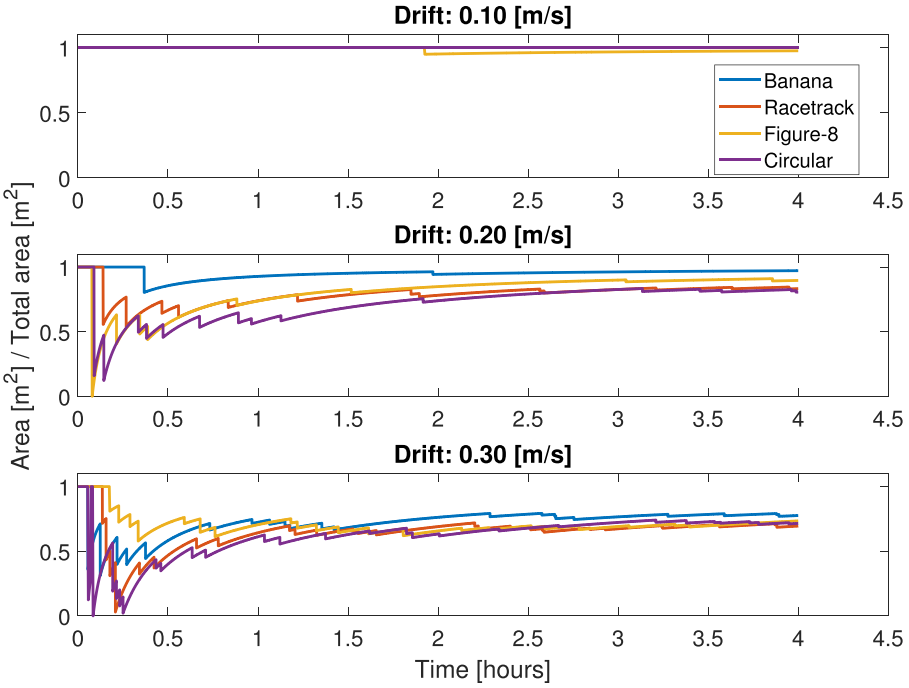

Fig. 18. KPI-FSULR (higher value is better).

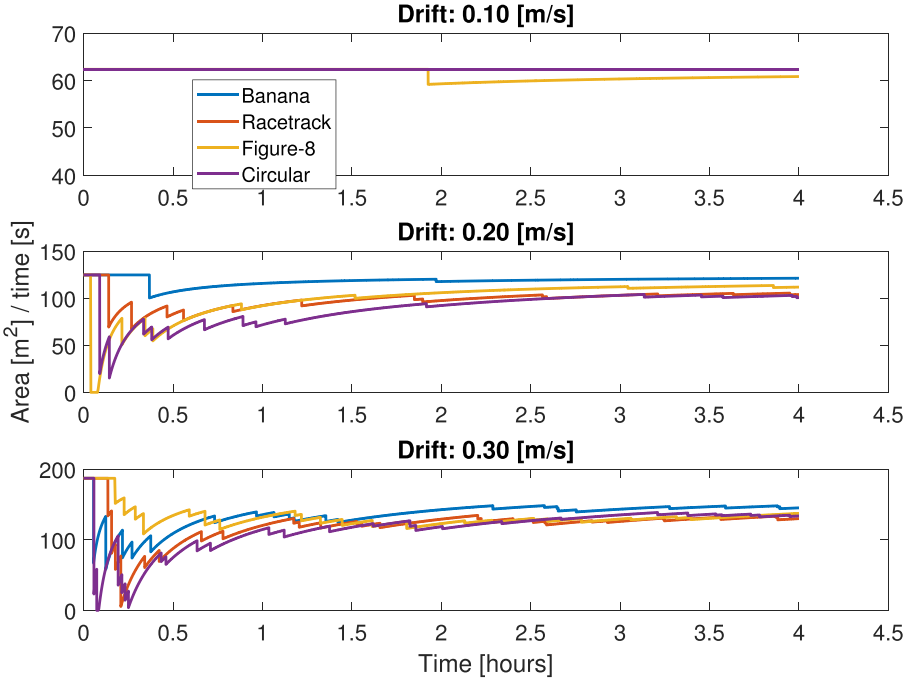

Fig. 19. KPI-ProdFloes (higher value is better).

efficient pattern according to the KPI-EffFloes as shown in Fig. 20. This compares the efficiency for the different patterns in terms of acceptable floe size production per energy unit of the icebreaker. The figure reveals the difference in floe size efficiencies, where we notice the best performance for the racetrack (higher velocities) and figure-8 (lower velocities) pattern. As for KPI-FSULR, these KPIs must also have a floe size detection system to be used in real operations.

4.3. *Performance of each pattern*

In the following discussion, the results in the text will be presented in 3-tuple arrays corresponding to the three ice drift speeds in the order {0.10 m/s, 0.20 m/s, 0.30 m/s}. By evaluating the different KPIs, we can identify trends for the different patterns.

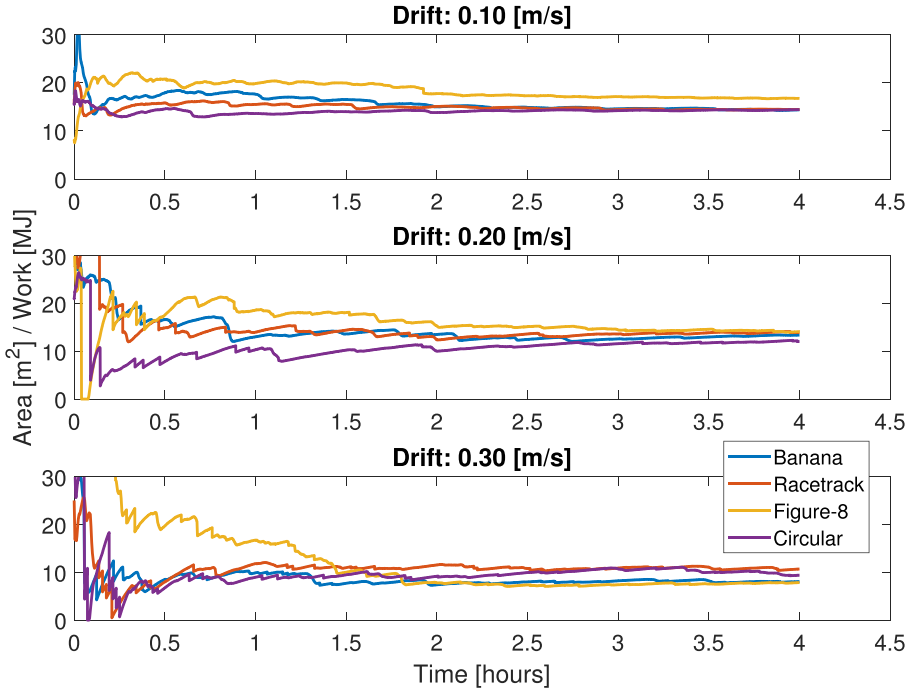

Fig. 20. KPI-EffFloes (higher value is better).

4.3.1. *Without IM*

In addition to simulations with IM, simulations without IM for the three ice drift velocities have been performed. For the non-IM results, the KPI-AMF had a mean load of {112482, 147385, 162708} kN, which are comparable to what one will get if using ISO standards (ISO/-FDIS/19906, 2019). Further, the KPI-ProdLoads ended up at {0.0145, 0.0060, 0.0007}. We observe from this that the loads increase from lower to higher drift velocities, which is the expected behavior. For load-based KPIs, we will discuss load reduction compared to the loads without IM. This is then calculated as (13).

$$\%\text{loadreduction} = \frac{\text{Load non-IM} - \text{LoadIM}}{\text{Load non-IM}} \times 100. \tag{13}$$

4.3.2. *Banana pattern*

Looking at the mean loads for the banana pattern in Fig. 14, we get the resulting KPI-AMF values {338, 1472, 5713} kN. The produced loads below threshold in Fig. 16 give the KPI-ProdLoads values for the banana pattern to stabilize at {1.0000, 0.9867, 0.5828} per time unit. Compared to the KPI-AMF results without IM it has a decrease of {99.70, 99.00, 96.49} % in load, and the loads kept under the limit have increased drastically compared to non-IM. Regarding the ice floes produced, we see from Figs. 18 and 19 that the floes reflect the loads, with KPI-FSULR values {1.0000, 0.9666, 0.7757} and KPI-ProdFloes at {62.370, 120.569, 145.137} m^2/s. From Fig. 13 we see that the work is the highest in all drift velocities, and consequently it has varying efficiencies presented in Figs. 17 and 20. The KPI-FSULR indicate that this pattern is the best to break the ice floes into small enough floes.

4.3.3. *Racetrack pattern*

The racetrack pattern achieves KPI-AMF of {591, 2089, 5050} kN. From Fig. 14, we see that the racetrack pattern has most of the time one of the lowest mean loads, and the KPI-ProdLoads values in Fig. 16 converges to {0.9726, 0.9494, 0.6179} per time unit. Compared to the KPI-AMF results of non-IM, it has a decrease of {99.21, 98.58, 96.90} %, and the loads kept under the limit have also increased significantly compared to non-IM. Looking at the floe areas in Fig. 19, the racetrack pattern creates acceptable floes with KPI-ProdFloes at {62.370, 103.812, 129.089} m^2/s. Fig. 18 yields that this pattern produces floes below threshold with KPI-FSULR at {1.0000, 0.8322, 0.6899}. Fig. 13 states that the racetrack pattern uses the least amount of work for the higher drift velocities, and this reflects into the efficiencies in Figs. 17 and 20.

4.3.4. *Figure-8 pattern*

From Fig. 14, we see that the figure-8 pattern has the highest mean load in the lowest drift velocity and get the lowest loads at the highest, with KPI-AMF values at {1264, 1561, 4626} kN. The production of loads below limit over time is also reflected by this, see Fig. 16, with KPI-ProdLoads values at {0.9341, 0.9832, 0.6265}. Compared to the KPI-AMF results of non-IM, it achieves a load reduction of {98.88, 98.94, 97.16} %, and the loads kept under the limit have increased significantly compared to non-IM. When looking at the change in momentum from Fig. 15, we observe some large loads that last for some time in the lowest drift velocity. The produced floes reflects the load scenario, where bigger floes create larger loads. From Fig. 19, we see that the figure-8 pattern produces floes below threshold of 150 m with KPI-ProdFloes areas at {60.550, 112.000, 131.357} m^2/s. Looking at Fig. 18, when the total area is accounted for, we see that the KPI-FSULR values are {0.9708, 0.8979, 0.7020}. From Fig. 13, we see that the pattern uses from least to almost the most amount of work. This is also reflected in Fig. 17, where it has efficient performance in the lowest drift speed, and the worst in the higher ones. In Fig. 20, we see that the pattern also has the worst efficiency when the floe sizes are accounted for in the highest drift velocity.

Table 3
Average of the last 30% values for each KPI, except for work where last value is used. The colors indicate the performance, going from better (green) to worse (red).

0.10 m/s

Track/KPI	KPI-Work	KPI-AMF	KPI-ILULR	KPI-ProdLoads	KPI-EffLoads	KPI-FSULR	KPI-ProdFloes	KPI-EffFloes	Score
Banana	62381	338	1.0000	1.0000	0.2339	1.0000	62.370	14.589	18
Racetrack	61992	591	0.6237	0.9726	0.2263	1.0000	62.370	14.510	13
Figure-8	52210	1264	0.4918	0.9341	0.2617	0.9708	60.550	16.947	9
Circular	62150	1022	0.9489	0.9939	0.2277	1.0000	62.370	14.290	13
Non-IM	-	112482	0.0000	0.0145	-	-	-	-	-

0.20 m/s

Track/KPI	KPI-Work	KPI-AMF	KPI-ILULR	KPI-ProdLoads	KPI-EffLoads	KPI-FSULR	KPI-ProdFloes	KPI-EffFloes	Score
Banana	130196	1472	0.9430	0.9867	0.1058	0.9666	120.569	12.935	17
Racetrack	107248	2089	0.8103	0.9494	0.1261	0.8322	103.812	13.791	12
Figure-8	114114	1561	0.9233	0.9832	0.1265	0.8979	112.000	14.410	18
Circular	120001	3847	0.4182	0.7478	0.0863	0.8195	102.222	11.804	1
Non-IM	-	147385	0.0000	0.0060	-	-	-	-	-

0.30 m/s

Track/KPI	KPI-Work	KPI-AMF	KPI-ILULR	KPI-ProdLoads	KPI-EffLoads	KPI-FSULR	KPI-ProdFloes	KPI-EffFloes	Score
Banana	258460	5713	0.2704	0.5828	0.0327	0.7757	145.137	8.156	10
Racetrack	174680	5050	0.3111	0.6179	0.0522	0.6899	129.089	10.896	16
Figure-8	251355	4626	0.2821	0.6265	0.0362	0.7020	131.357	7.599	13
Circular	204324	6912	0.1930	0.4391	0.0337	0.7223	135.144	10.350	9
Non-IM	-	162708	0.0000	0.0007	-	-	-	-	-

4.3.5. Circular pattern

Ultimately, the circular pattern produces high mean load values in all ice drift velocities, as seen from Fig. 14, with KPI-AMF values at {1022, 3847, 6912} kN. It produces loads that are under the limit the least of the time with KPI-ProdLoads values at {0.9939, 0.7478, 0.4391}. Compared to the results without IM, it has a decrease in KPI-AMF of {99.09, 97.39, 95.75} %, and the loads are kept under the limit longer than non-IM. It produces acceptable KPI-ProdFloes areas with values of {62.370, 102.222, 135.144} m^2/s (Fig. 19). The pattern have a varying number of approved floes in the different drift velocities, see Fig. 18, with KPI-FSULR values at {1.0000, 0.8195, 0.7223}. Accounting for the varying work seen in Fig. 13, the efficiencies are slightly lower in Figs. 17 and 20 with some exceptions.

4.4. Overall comparison of the patterns

Table 3 presents the average numbers of the last 30% samples for each KPI, except for work where last value is used. Here are also the simulations without IM included, to directly illuminate the effective load reduction of each pattern. In addition to this, a simple score has been added to quickly highlight the better performing track. This indicates how many times a particular pattern has better performance in the different KPIs. It is calculated by simply assigning the best results 3 points, second best result 2 points, thereafter 1 point, and 0 point for worst performance. This is obviously a very coarse weighted sum of the different KPIs. For the simulation-based planning of a real operation, the decision team should determine the weighting of the different KPIs based on the important criteria for the operation.

As an overall observation, the different patterns have both strengths

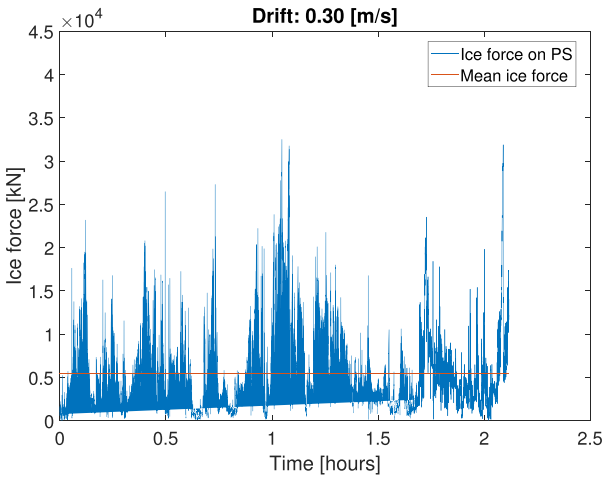

Fig. 21. Ice load on PS, original simulation with IB close to PS.

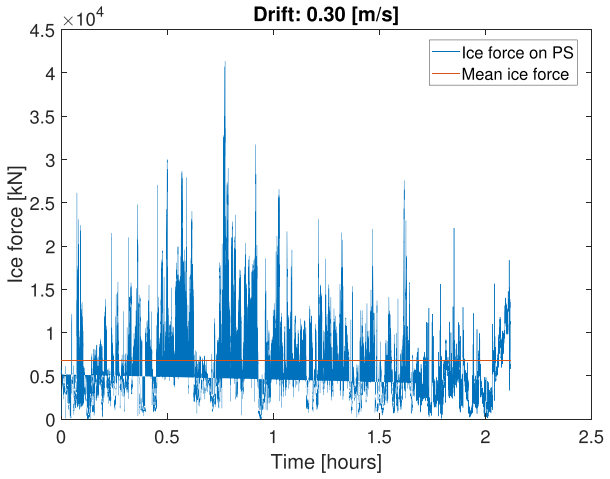

Fig. 22. Ice load on PS, new simulation with IB further away from PS.

and weaknesses in the presented KPIs. The best pattern is perhaps the banana-shaped, as observed in Table 3, due to its consistently high scores in most KPIs, but it suffers from larger energy consumption. The racetrack pattern has the best KPI performance in the highest drift velocity, but it suffers some in slower velocities. The circular pattern has a low performance in most KPIs, and it suffers from the production of larger loads and ice floes. The figure-8 pattern has overall a good performance in the KPIs of this simulation study, and it is the best pattern with ice drift velocity at 0.2 m/s.

We will not conclude that a certain pattern is better than the others in this study, as different setups and parameters can change the outcome. The study serves to demonstrate the evaluation of planned icebreaker performance in specified conditions, to illustrate the information provided by the proposed KPIs, and to trigger new ideas on how to address performance of physical IM. Comparing the suggested KPIs with the traditional floe size distribution used as performance indicator, we find that the new ones give a broader insight of the differences between the different patterns. For instance, when comparing two operations based on a single KPI, it is easy to prejudge one operation as favorable. However, when comparing with another KPI, e.g. the applied energy, the earlier conclusion may change. When the results are also compared against those of non-IM we see, as expected, huge advantages of including IM for load reduction.

4.5. Remarks on the simulations

Snapshots from the different simulations at certain timestamps can be found in Appendix A; Figs. 23, 24, 25 and 26. From these snapshots it can be seen that the ice floes are kept confined and that the measures, mentioned in Section 3.5 to do this, work. The deletion of floes reduces the computation time noticeably, and it seems necessary as the body count increases a lot when the IB manages the ice up front of the PS. The way this function is implemented does not influence the ice load results recorded on the PS. As mentioned earlier, high-fidelity simulations take time; hence, to shorten the simulation time by other methods is being investigated.

The method used to decrease the simulation time was to move the IB closer to the PS. To check if the PS was influenced by the IB, a new simulation where the IB was moved further away from the PS using the same IB pattern, was performed. Comparing the results from these two simulations, seen in Figs. 21 and 22, we observed that the mean ice load is increasing when the IB is further away. Studying the visual results, we observed that some of the peaks from the original simulation (Fig. 21) came from a chain of ice floes that occurs between the IB and PS; however, most of the peaks were traced back to larger floes hitting the PS. The ice floe chains were not observed in the simulation with the IB further away, and the peaks here only originated from larger floes hitting the PS. From this, we conclude that the distance between the IB and PS is a topic to be carefully considered when verifying planned IM operations.

5. Conclusion

This paper demonstrated the use of high-fidelity simulations to evaluate different IM strategies. Furthermore, it has demonstrated the use of KPIs other than ice floe sizes to provide deeper insight into the performance of the different icebreaker operations in IM under various test conditions. To conclude on the performance of the different patterns, we see that all of the patterns vary in performance in the KPIs for the different ice drift speeds. The banana and racetrack patterns seem to perform best in most evaluations, with figure-8 just behind.

In future applications, the methods in this paper can be used to set up simulations for free floating icebreakers (under investigation) with actively controlled and limited capacity propulsion systems. This can then be used to evaluate the KPIs resulting from various icebreaker operational strategies and setups, as well as a greater variability in ice conditions, in order to gain deeper insight and develop better control and decision support functions for icebreaker operations. Such studies can be extended with sensitivity analysis in the most important parameters to determine safety factors and contingencies. One should note, though, that the computational cost is still high, and a highly increased simulation scope may at some point become impractical – improving the computational complexity without losing fidelity is ongoing research.

Declaration of Competing Interest

The authors declare no conflict of interest.

Acknowledgments

The Oden Arctic Technology Research Cruise 2015 (OATRC2015) was performed by the Norwegian University of Science and Technology (NTNU) in cooperation with the Swedish Polar Research Secretariat (SPRS) and the Swedish Maritime Administration (SMA), with support from the ExxonMobil Upstream Research Company. This work was also supported by the Research Council of Norway through two projects; CRI SAMCoT, RCN prj. no. 203471, and partly through the Centre of Excellence NTNU AMOS, RCN prj. no. 223254.

Appendix A. Additional figures

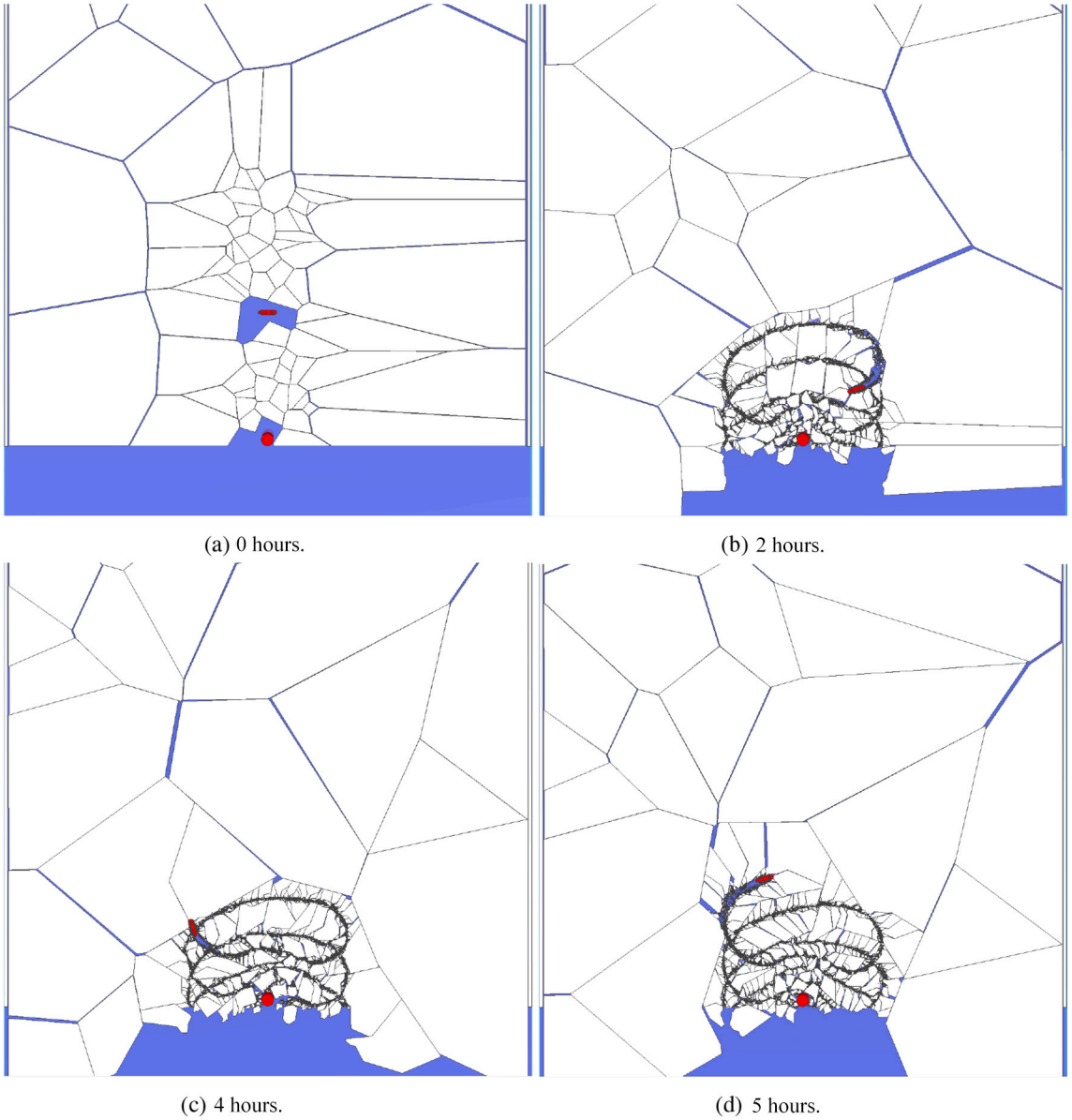

Fig. 23. Screenshots of IM simulation, banana pattern, 0.20 m/s ice drift. (a) 0 hours. (b) 2 hours. (c) 4 hours. (d) 5 hours.

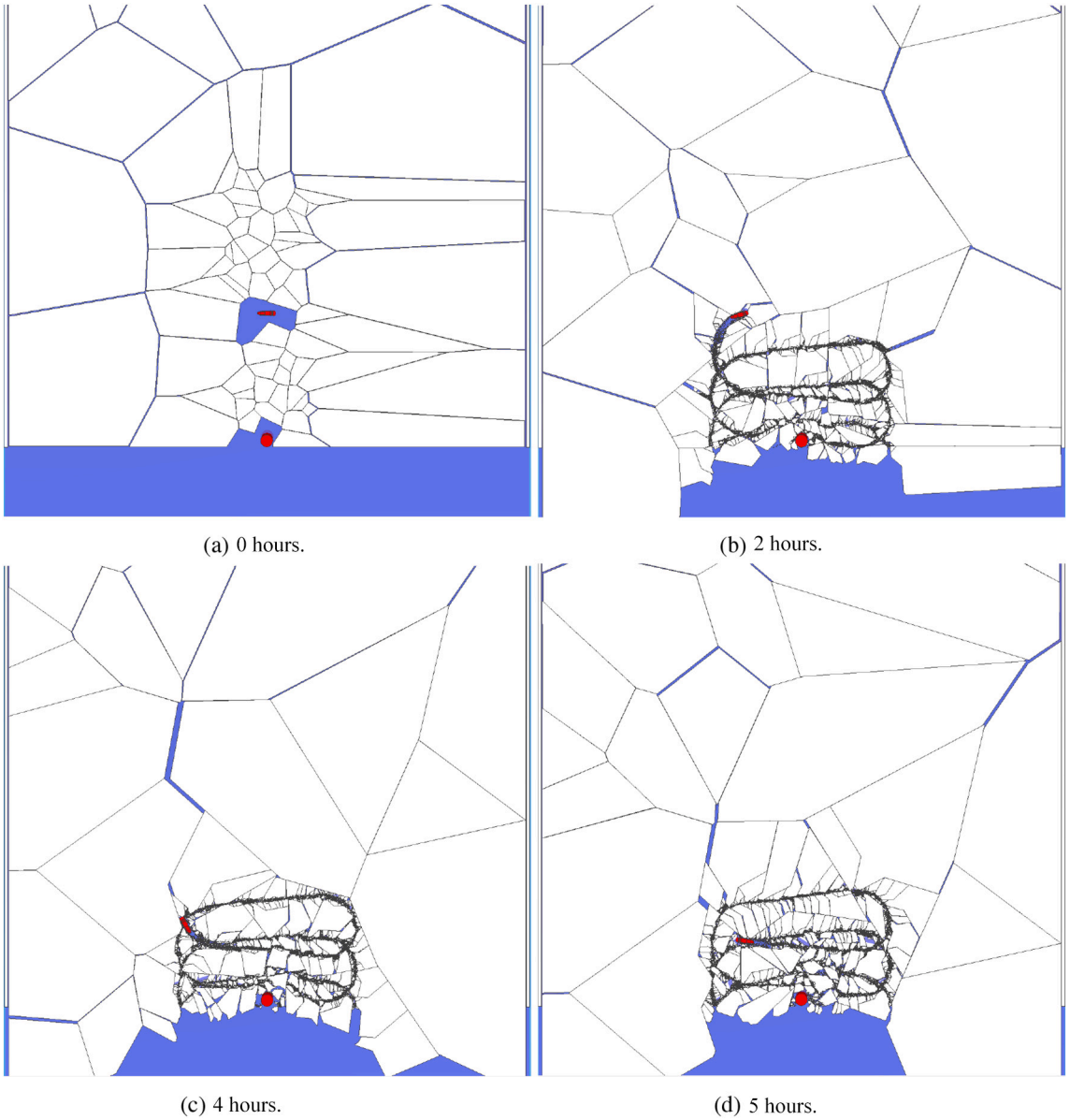

Fig. 24. Screenshots of IM simulation, racetrack pattern, 0.20 m/s ice drift. (a) 0 hours. (b) 2 hours. (c) 4 hours. (d) 5 hours.

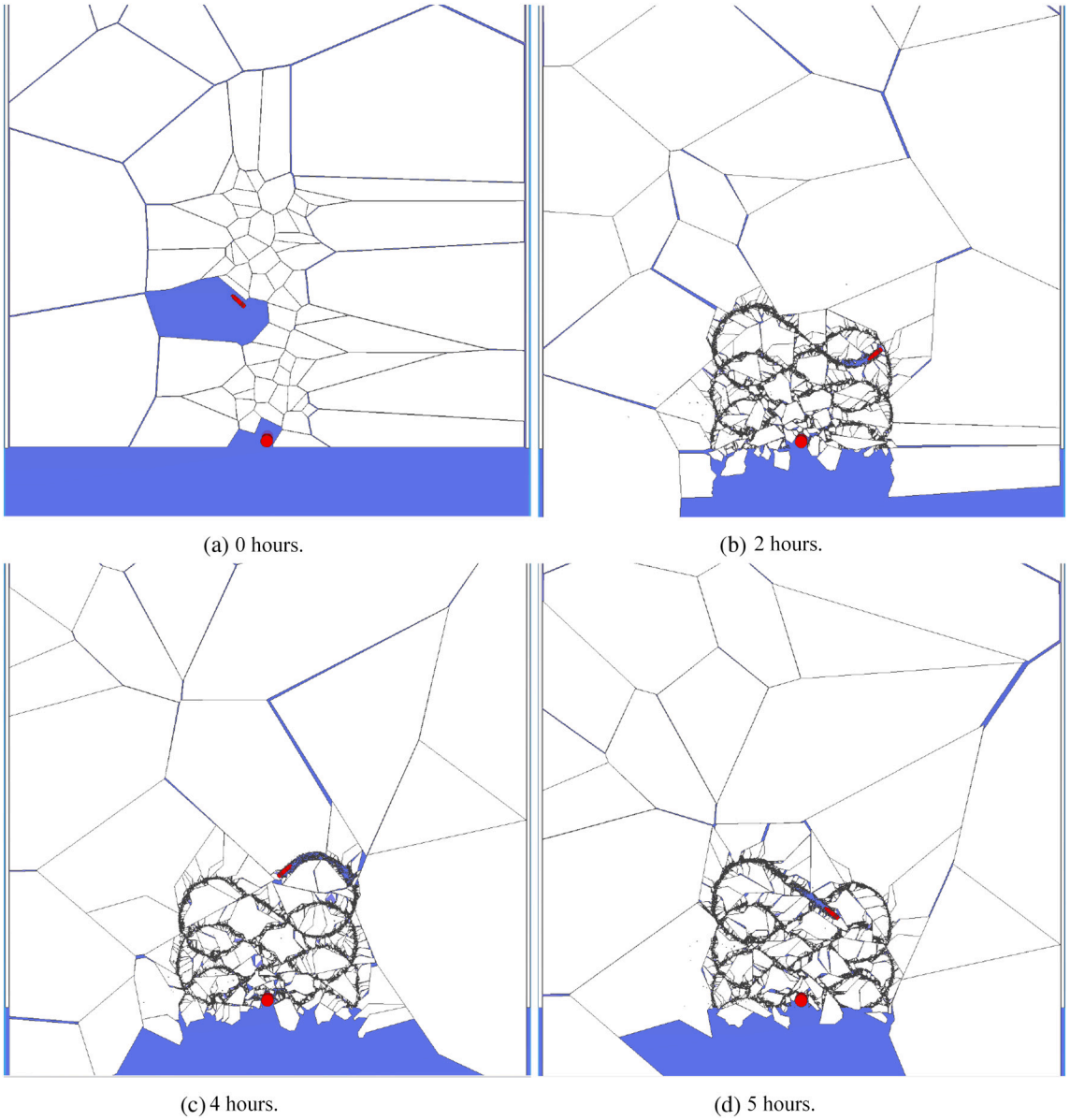

Fig. 25. Screenshots of IM simulation, Figure-8 pattern, 0.20 m/s ice drift. (a) 0 hours. (b) 2 hours. (c) 4 hours. (d) 5 hours.

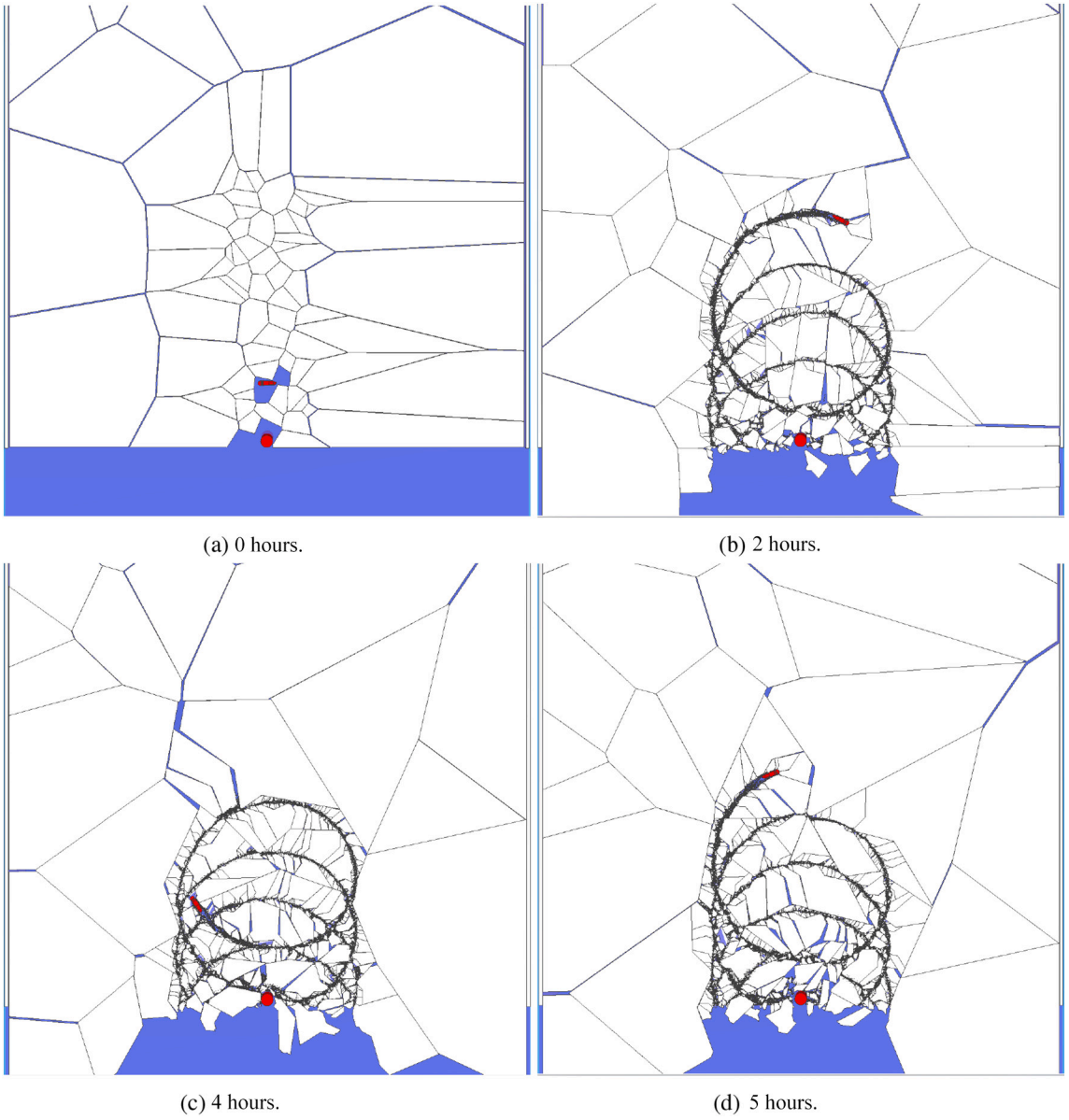

Fig. 26. Screenshots of IM simulation, circular pattern, 0.20 m/s ice drift. (a) 0 hours. (b) 2 hours. (c) 4 hours. (d) 5 hours.

References

Backman, J., Moran, K., Evans, D., the Expedition 302 Project Team, 2004, 2004. ACEX – Arctic Coring Expedition: paleoceanographic and tectonic evolution of the central Arctic Ocean. IODP Sci. Prosp. 302 https://doi.org/10.2204/iodp.sp.302.2004.

Blender Foundation, 2018. Blender [Software]. https://www.blender.org/.

DELFTShip Maritime Software, 2018. DELFTShip Free [Software]. https://www.delftship.net/DELFTwp/delftship/.

Eik, K.J., 2010. Ice Management in Arctic Offshore Operations and Field Developments, PhD thesis. Norwegian University of Science and Technology (NTNU), Trondheim, Norway.

Hamilton, J.M., 2011. The challenges of deep-water arctic development. Int. J. Offshore Pol. Eng. 21 (4), 241–247.

Hamilton, J.M., Holub, C., Blunt, J., 2011a. Simulation of Ice Management Fleet Operations Using Two Decades of Beaufort Sea Ice Drift and Thickness Time Histories. In: Proceedings of International Society of Offshore and Polar Engineers (ISOPE). International Society of Offshore and Polar Engineers, Maui, Hawaii.

Hamilton, J.M., Holub, C., Blunt, J., Mitchell, D., Kokkinis, T., 2011b. Ice management for support of arctic floating operations. In: OTC Arctic Technology Conference. Offshore Technology Conference. https://doi.org/10.4043/22105-ms.

Heyn, H.-M., Knoche, M., Zhang, Q., Skjetne, R., 2017. A system for automated vision-based sea-ice concentration detection and floe-size distribution indication from an icebreaker. In: Volume 8: Polar and Arctic Sciences and Technology Petroleum Technology. American Society of Mechanical Engineers. https://doi.org/10.1115/omae2017-61822.

Holub, C., Matskevitch, D., Kokkinis, T., Shafrova, S., December 2018. Near-field ice management tactics – simulation and field testing. Cold Regions Science and Technology 156, 23–43. https://doi.org/10.1016/j.coldregions.2018.02.003.

ISO/FDIS/19906, 2019. Petroleum and Natural Gas Industries - Arctic offshore structures. International standard, International Organization for Standardization, Geneva, Switzerland.

Johansson, B.M., Liljestrom, G.C., 1989. ODEN - a state-of-the-art icebreaker.. In: POAC '89: Proceedings of the 10th International Conference on Port and Ocean Engineering under Arctic Conditions, volume 3. Luleaa, Sweden, pp. 1229–1265.

Kjerstad, Ø.K., Skjetne, R., Berge, B.O., 2013. Constrained nullspace-based thrust allocation for heading prioritized stationkeeping of offshore vessels in ice. In: Int. Conf. Port Ocean Eng. Arctic Conditions, Espoo, Finland.

Lu, P., Li, Z.J., Zhang, Z.H., Dong, X.L., 2008. Aerial observations of floe size distribution in the marginal ice zone ofsummer Prydz Bay. J. Geophys. Res. 113 (C02011) https://doi.org/10.1029/2006JC003965.

Lu, W., 2014. Floe Ice - Sloping Structure Interactions. PhD thesis. Norwegian University of Science and Technology, Trondheim, Norway.

Lu, W., Lubbad, R., Løset, S., 2015. Tentative fracture mechanisms of the parallel channel effect during ice management. In: Proceedings of the International Conference on Port and Ocean Engineering Under Arctic Conditions.

Lu, W., Lubbad, R., Løset, S., Skjetne, R., 2016a. Parallel channel tests during ice management operations in the arctic ocean. In: Arctic Technology Conference. Offshore Technology Conference. https://doi.org/10.4043/27344-ms.

Lu, W., Zhang, Q., Lubbad, R., Løset, S., Skjetne, R., 2016b. A shipborne measurement system to acquire sea ice thickness and concentration at engineering scale. In: Arctic Technology Conference. Offshore Technology Conference. https://doi.org/10.4043/27361-ms.

Lu, W., Heyn, H.-M., Lubbad, R., Løset, S., 2018a. A large scale simulation of floe-ice fractures and validation against full-scale scenario. Int. J. Naval Architect. Ocean Eng. 10 (3), 393–402. https://doi.org/10.1016/j.ijnaoe.2018.02.006.

Lu, W., Lubbad, R., Løset, S., 2018b. Parallel channels fracturing mechanism during ice management operations. part II: experiment. Cold Reg. Sci. Technol. 156, 117–133. https://doi.org/10.1016/j.coldregions.2018.07.011.

Lu, W., Lubbad, R., Shestov, A., Løset, S., 2018c. Parallel channels fracturing mechanism during ice management operations. part i: theory. Cold Reg. Sci. Technol. 156, 102–116. https://doi.org/10.1016/j.coldregions.2018.07.010.

Lubbad, R., Løset, S., Lu, W., Tsarau, A., van den Berg, M., December, 2018. An overview of the Oden arctic technology research cruise 2015 (OATRC2015) and numerical simulations performed with SAMS driven by data collected during the cruise. Cold Regions Science and Technology 156, 1–22. https://doi.org/10.1016/j.coldregions.2018.04.006.

Lubbad, R., Løset, S., Lu, W., Tsarau, A., van den Berg, M., 2018b. Simulator for arctic marine structures (SAMS). In: Volume 8: Polar and Arctic Sciences and Technology Petroleum Technology. ASME. https://doi.org/10.1115/omae2018-78592.

Palmer, A., Croasdale, K.R., 2012. Arctic Offshore Engineering. World Scientific Publishing Company, Singapore. ISBN 9814368776.

Raza, N., van den Berg, M., Lu, W., Lubbad, R., 2019. Analysis of Oden icebreaker performance in level ice using simulator for arctic marine structures (SAMS). In: Proceedings - International Conference on Port and Ocean Engineering under Arctic Conditions, Delft, The Netherlands.

Swedish Maritime Administration, 2013. Icebreaker Oden: Main Particulars, Machinery, and Vessel Details. Swedish Maritime Administration, Sweden. https://sjofartsverket.se/globalassets/isbrytning/isbrytarbilder/oden-for-webben.pdf. Technical report.

Toyota, T., Takatsuji, S., Nakayama, M., 2006. Characteristics of sea ice floe size distribution in the seasonalice zone. Geophys. Res. Lett. 33 https://doi.org/10.1029/2005gl024556. L02616.

Tsarau, A., van den Berg, M., Lu, W., Lubbad, R., Løset, S., 2018. Modelling results with a new simulator for arctic marine structures - SAMS. In: Volume 8: Polar and Arctic Sciences and Technology Petroleum Technology. American Society of Mechanical Engineers. https://doi.org/10.1115/omae2018-78593.

Tuhkuri, J., Polojärvi, A., 2018. A review of discrete element simulation of ice–structure interaction. Philos. Trans. Royal Soc.: Math. Phys. Eng. Sci. 376 (2129), 20170335. https://doi.org/10.1098/rsta.2017.0335.

van den Berg, M., Lubbad, R., Løset, S., 2019. The effect of ice floe shape on the load experienced by vertical-sided structures interacting with a broken ice field. Marine Struct. 65, 229–248. https://doi.org/10.1016/j.marstruc.2019.01.011.

van den Berg, M., Bjørnø, J., Lu, W., Skjetne, R., Lubbad, R., Løset, S., 2021. The value of high-fidelity numerical simulations of ice-ship and ice-structure interactions in arctic design with informed decision making. In: Berkman, P.A. (Ed.), Informed Decisionmaking for Sustainability. Volume 2. Building Common Interests in the Arctic Ocean with Global Inclusion. Springer. Accepted.

Zhang, Q., Skjetne, R., 2015. Image processing for identification of sea-ice floes and the floe size distributions. IEEE Trans. Geosci. Rem. Sens. 53 (5), 2913–2924. https://doi.org/10.1109/tgrs.2014.2366640.